University of Stavanger

**Faculty of Science and Technology**
**Department of Mechanical and Structural Engineering and Materials Science**

# Optimization of Airfoil Shape for a Bidirectional Tidal Stream Turbine

Master's Thesis in Master of Science in Engineering Structures and Materials

by

Ghazal Sadat Shariatpanahi

Internal Supervisor

Knut Erik Teigen Giljarhus

June 14, 2021

*"And then one day you find ten years have got behind you.*
*The sun is the same in a relative way but you're older"*

Pink Floyd - Time

# Abstract

A tidal turbine design needs to consider the harsh environment of the sea. Reducing the number of moving parts is therefore desirable. A tidal stream is relatively predictable with small directional variance. To avoid a yaw gear an attractive option is to instead use a reversible airfoil, allowing the turbine to operate in both ebb and tide. This work investigates various reversible airfoil designs and airfoil optimization. The airfoils are based on existing NACA 6 profiles and profiles using B-spline parameterization. The optimization process showed that it is challenging to obtain a profile that has both good lift and good aerodynamic effectiveness as these two parameters are opposing each other. Still, a viable design is obtained that has improved performance compared to the simpler design based on modifying a NACA 6 profile.

# Acknowledgements

I would like to express my deepest thanks:

To my dear supervisor, Knut Erik Teigen Giljarhus, my great teacher and support during this thesis. Thank to him for his encouragement, help, advice and patience; without which, I would not have been able to complete this research. A huge thanks to him for giving me hope and always being on my side.

To the faculty of science and technology at UiS, for giving me this outstanding chance to be able to be part of this amazing master program; which has helped me broaden and increase my knowledge, motivation and belief for being a great mechanical engineer to the world.

To my lovely family and friends whom their supports always motivated me.

# Contents

# Abbreviations

| | |
|---|---|
| **NACA** | **N**ational **A**dvisory **C**ommittee for **A**eronautics |
| **CFD** | **C**omputational **F**luid **D**ynamics |
| **RANS** | **R**eynolds **A**veraged **N**avier **S**tokes |
| **TCT** | **T**idal **C**urrent **T**urbine |
| **y+** | **y** **P**lus |

# Symbols

| Latin Symbol | Name | Unit |
|---|---|---|
| $a$ | Distance | m |
| $C$ | Wind Area | $m^2$ |
| $C_D$ | Drag Coefficient | |
| $C_L$ | Lift Coefficient | |
| $F_D$ | Drag Force | N |
| $F_L$ | Lift Force | N |
| $P$ | Power | W ($Js^{-1}$) |
| $U_\infty$ | Free Stream Velocity | m/s |

| Greek Symbol | Name | Unit |
|---|---|---|
| $\rho$ | Density | $kg/m^3$ |
| $\omega$ | Angular Frequency | $rads^{-1}$ |

# Chapter 1

# Introduction

The energy demand is increasing gradually as population grow. Currently, this energy severely depends on fossil fuels, which is not a good choice for environment. Fossil fuels are the main source of CO2 emissions. Hence, the more fossil fuels are burnt to provide energy, the more CO2 in the atmosphere, which results in a green house effect and increasing temperatures on Earth [1].

To address this problem, it is important to use another source of energy which not only has minimum environmental effects, but also is renewable [1]. Some examples of renewable energy are; Wind power, solar power, biomass energy and tidal energy. While wind and solar energies are widely used, tidal power is currently not as widespread [2, 3].

The proper history of considering the ocean current energy for power generation, starts after the first oil crises in 1970. During years between 1970 and 1990 the UK had a vital role in introducing the tidal power as a ocean energy and developing turbines. Main study and work on this type of energy and turbines is done in UK, Norway, Canada, USA, Australia and France [4]. In 1980, more than a thousand patents were registered for converting wave energy into power [2]. However, the ideal of utilizing ocean energy is very old. One of the initial patents was recorded by a Frenchman and his son Girard in 1799.

In order to harvest the energy from ocean and tides, many devices are being concerned and most of them are designed around horizontal and vertical axis turbine, which generates electricity from tides. Since then, many investigations have been done regarding to design and operation effective parameters [2].

Tidal power, also referred as tidal energy, is a unlimited source of energy which comes from tides in ocean [5]. Energy from tides is mostly captured during the rise and fall of the sea level. Tides can be divided into vertical water movement (rise and fall) and horizontal

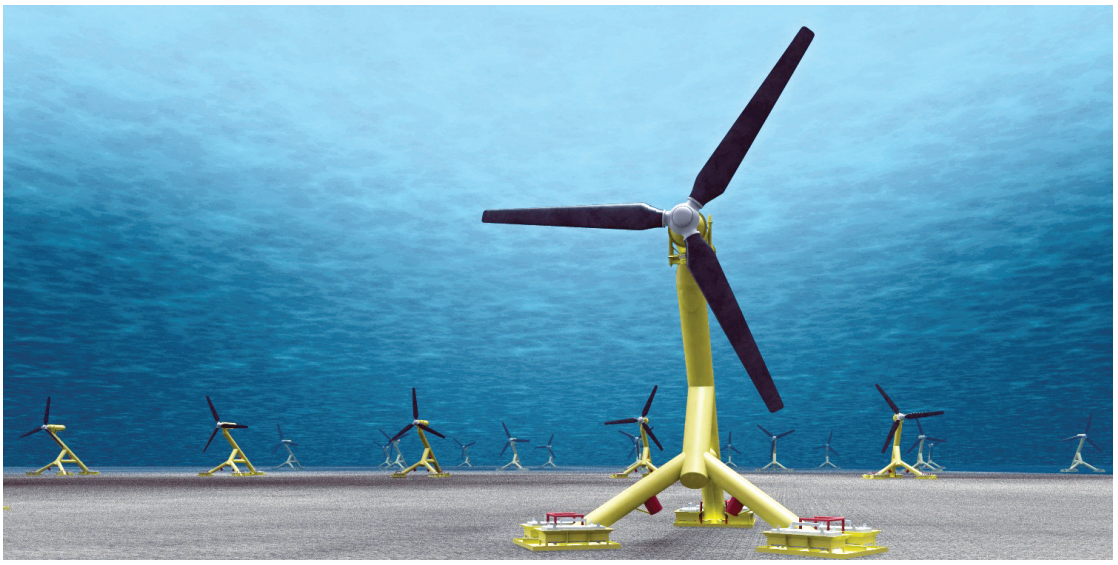

**Figure 1.1:** Example of Horizontal Tidal Turbine [2].

water movement (tidal current). The difference is that vertical movement is the difference between high and low tide (potential energy) but tidal current is the horizontal water movement (kinetic energy). Present developments are based on tidal current which utilize the kinetic energy. The growing interest in exploring tidal current technologies has many compelling reasons such as environment friendly nature, intermittent but predictable, security and diversity of supply and limited social and environmental impacts. The fact is that oceans cover more than 70 percent of the earth's surface which obviously indicates the enormous resources of ocean energy. The tidal stream is also more predictable than wind giving more stable energy production. Finally, the higher density of water compared to air means higher energy production per surface area.

The are two most common methods of tidal current energy extraction are horizontal and vertical axis tidal current turbines . In a horizontal design, see Figure 1.1, the turbine blades rotate about a horizontal axis which is parallel to the direction of the flow of water. In a vertical design, the turbine blades rotate about a vertical axis which is perpendicular to the direction of the flow of water.

Regardless of the orientation of the blades, the blade profile should be optimized to extract the most energy from the flow. For a vertical design, the direction of the tidal current does not impact the performance of the turbine. For a horizontal one, however, the flow direction will be important. Since the tidal ebb and tide is predictable, a simplified design where the blades are reversible is attractive. This thesis will investigate how a reversible blade should be designed, and the trade-off in performance relative to a single-direction blade.

# Chapter 2

# Materials and methods

## 2.1 Definitions

For the airfoil, the forces acting upon it are divided into two components; the drag, which acts in the direction parallel to the incoming flow and the lift, which acts in the direction perpendicular to the incoming flow.

The forces are typically made non-dimensional in the form of drag and lift coefficients. These are defined as

$$C_D = \frac{F_D}{\frac{1}{2}\rho U_\infty^2 C} \tag{2.1}$$

$$C_L = \frac{F_L}{\frac{1}{2}\rho U_\infty^2 C}, \tag{2.2}$$

where $F_D$ and $F_L$ are the forces in the drag and lift directions, respectively, $\rho$ is the fluid density, $U_\infty$ is the freestream velocity and $C$ is the planform wind area.

## 2.2 Airfoil geometry

This section presents the different airfoils considered in this study.

### 2.2.1 Baseline airfoil, NACA65-415

The baseline airfoil used for comparison is the uni-directional NACA 65-415 airfoil. NACA airfoils represent airfoil shapes using a series of digits, which represent the airfoil

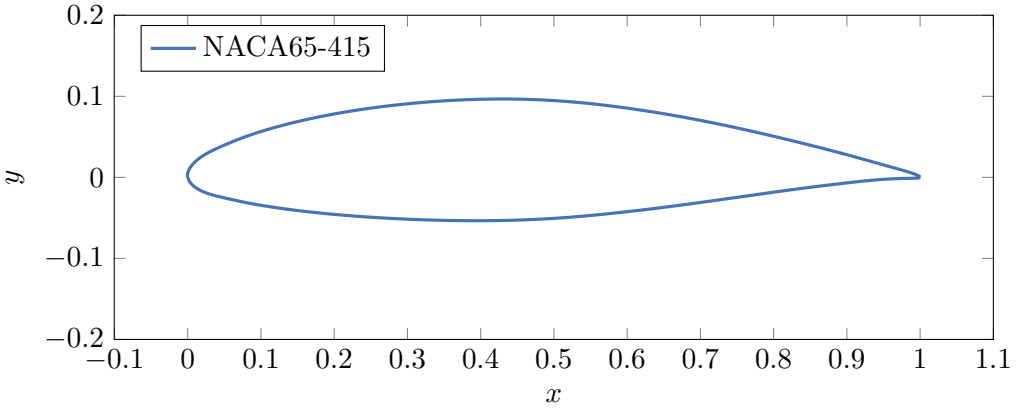


**Figure 2.1:** Geometry of the baseline airfoil, NACA 65-415.

section's critical geometric properties. During late 1920s and 1930s, NACA developed a series of tested airfoils and devised a numerical designation for each airfoil. . For instance NACA65-415, which used in this project, can be described as: 6, designates the series. 5, is the location of the minimum pressure in tenths of chord (0.5c). 4, means that the design lift coefficient is 0.4. The last two digits shows the thickness in percentage of chord, 15. This airfoil can be seen in Figure 2.1.

### 2.2.2 Elliptic airfoil

The elliptic airfoil is defined using the formula for an ellipse,

$$\frac{x^2}{a^2} + \frac{y^2}{b^2} = 1, \tag{2.3}$$

where $a$ and $b$ are the major and minor axes, respectively. Here, the thickness is 15 %, same as the baseline airfoil, and use the default airfoil chord length of one, giving

$$y = \frac{3\sqrt{1 - x^2}}{40} \tag{2.4}$$

### 2.2.3 NACA symmetric airfoil, SYM65-015

This geometry is a bisymmetric version of the baseline airfoil. The first 40 % of the upper leading edge is mirrored around the $y$-axis at the half chord length and then mirrored again around the $x - axis$. The two parts are finally connected by a straight line. The resulting profile is shown in Figure 2.2, together with the elliptic airfoil. It is clear that the two profiles are very similar.

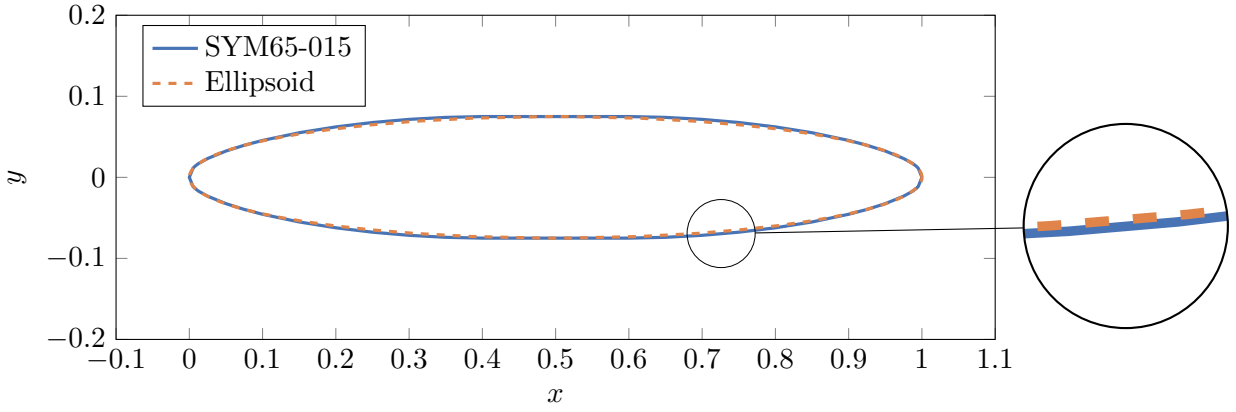


**Figure 2.2:** Geometry of the SYM65-015 airfoil, compared against the ellipsoid airfoil.

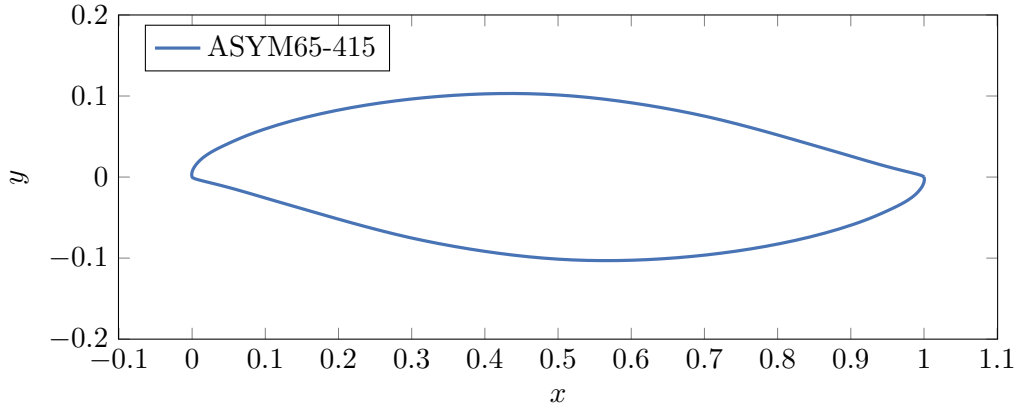


**Figure 2.3:** Geometry of the reversible, asymmetric version of the NACA 65-415, where the upper profile is rotated to generate the lower profile.

### 2.2.4 NACA reversible airfoil, REV65-415

The final case is the asymmetric NACA profile built by taking the NACA 65-415 profile for the upper profile, then flipping that profile both vertically and horizontally to generate the lower part. The resulting profile is shown in Figure 2.3. Note that due to the camber of the original profile, this version will be significantly thicker than the original airfoil at the half chord length.

### 2.2.5 B-spline parameterized airfoil

There are many different way to parameterize an airfoil for use in optimization. Convergence rate, minimum existing parameters and range of airfoil that can be represented are three important factors which should be considered. In [6], a review of these techniques are given. Regardless of which technique is considered, they should minimize the number of parameters and be able to cover a wide range of existing airfoils.

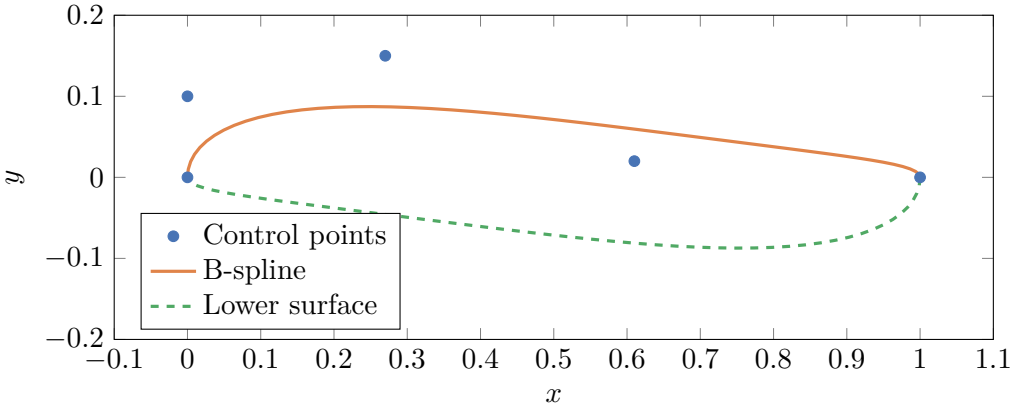


**Figure 2.4:** Illustration of control points and B-spline used for airfoil shape parameterization.

In this work, the technique used in [7] is adopted. The airfoil is parameterized by a sixth degree B-Spline using six control points, as shown in Figure 2.4. The end points are fixed to (0,0) and (1,0), and the second and second to last points are only allowed to move along the $y$-axis. This gives a total of six parameters for a single airfoil realization.

## 2.3 Optimization

Generally speaking, optimization means to find the minimum of an objective function, potentially given some constraints. There are different techniques available depending on the behavior of the objective function, and whether there are constraints or not. There are also techniques for multi-disciplinary optimization, where different disciplines have different objective functions. This could be for instance combining the aerodynamic performance of and airfoil and its structural behavior. As part of the search for the optimum point, the objective function must be evaluated multiple times.

As computers have become increasingly powerful, the possibility to use optimization techniques have become more of a reality. However, there are inherent issues with optimization that are important to consider. Already in 1998, Drela discussed pros and cons of airfoil optimization. As for airfoil parameterization, there are also multiple techniques to optimize its design [7].

In this work, methods from the `optimize` package of SciPy are used. For unconstrained optimization, the Simplex method is chosen [9].

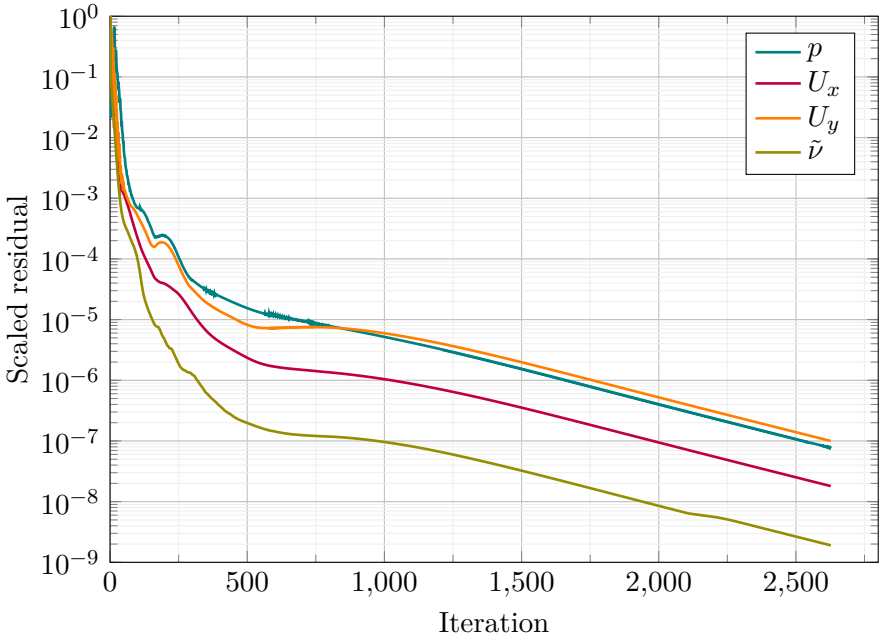


**Figure 2.5:** Example residual plot for the medium grid demonstrating typical convergence behaviour.

## 2.4 Computational fluid dynamics

In computational fluid dynamics, the governing equations for fluid flow are solved numerically. This offers a generic way of tackling a wide variety of fluid flow problems. The fluid domain is divided into smaller cells and discrete approximations are introduced for the continuous terms of the equations. Also, due to the inherent complexity of turbulence, turbulence models are typically used. Meanwhile, Using CFD technique for evaluation of TCT is widely used [10]. The simulations in this work were performed in the open-source CFD simulation software OpenFOAM, version 7 [11, 12].

Simulations were performed with a Reynolds-averaged Navier-Stokes (RANS) turbulence model, more specifically the Spalart-Allmaras turbulence model [13]. The SIMPLE algorithm was used for pressure-velocity coupling. For discretization, second-order discretization schemes are used for spacial discretization. For the convective terms, a second-order central-upwind scheme with a Sweby limiter was used [14]. The residual limit for the solution process was set to $1 \times 10^{-6}$ for all variables. Figure 2.5 shows the typical convergence behavior of the simulations.

### 2.4.1 Computational Mesh

Construct2D is an elliptic grid generator to create 2D grids for CFD computations on airfoils. The only required input file is the set of coordinates defining the airfoil geometry.

Construct2D can create grids for both airfoils with a blunt trailing edge and airfoils with a sharp trailing edge. The grids are generated in Plot3D format, which can then be converted to the OpenFOAM grid format.

The overall computational domain as well as the mesh close to the airfoil is shown in Figure 2.6. The mesh is an O-grid with radius 25 times the chord length of the airfoil.

### 2.4.2 Mesh sensitivity

A mesh study was performed to find a suitable grid for the remainder of the work. Since the aim is to use the CFD simulation in an optimization process, a good compromise between simulation speed and accuracy is required.

Table 2.1 shows the mesh parameters and the resulting drag/lift coefficients. The grids are made by successively increasing all the mesh parameters; the number of points on the airfoil surface, the mesh spacing near the edges and the number of points in the fluid volume.

There is minor differences between coarse, medium and fine grids, indicating that the medium mesh size is sufficient. A single simulation with this grid only takes around 30 seconds, running on an Intel Xeon Gold 6148 processor with 20 2.4 GHz cores.

**Table 2.1:** Sensitivity of mesh size.

| Grid | Surface points | Edge spacing | Volume points | Drag | Lift |
|---|---|---|---|---|---|
| Very coarse | 125 | $4 \times 10^{-3}$ | 50 | 0.02757 | 0.3822 |
| Coarse | 188 | $3 \times 10^{-3}$ | 75 | 0.02697 | 0.3849 |
| Medium | 250 | $2 \times 10^{-3}$ | 100 | 0.02673 | 0.3861 |
| Fine | 375 | $1.5 \times 10^{-3}$ | 150 | 0.02658 | 0.3868 |

Another important parameter for the mesh is the distance from the airfoil to the first grid cell. This is often expressed in non-dimensional coordinates, and denoted $y^+$. For the Spalart-Allmaras turbulence model, this should be close to unity, in order to fully resolve the turbulent boundary layer near the airfoil. Table 2.2 shows the results of varying this parameter. There is some variation from 4 to 2, but no difference from 2 to 0.9. Hence, $y^+ = 2$ was chosen for this work.

**Table 2.2:** Sensitivity of $y^+$.

| $y^+$ | Drag | Lift |
|---|---|---|
| 4 | 0.02687 | 0.3868 |
| 2 | 0.02673 | 0.3861 |
| 0.9 | 0.02673 | 0.3861 |

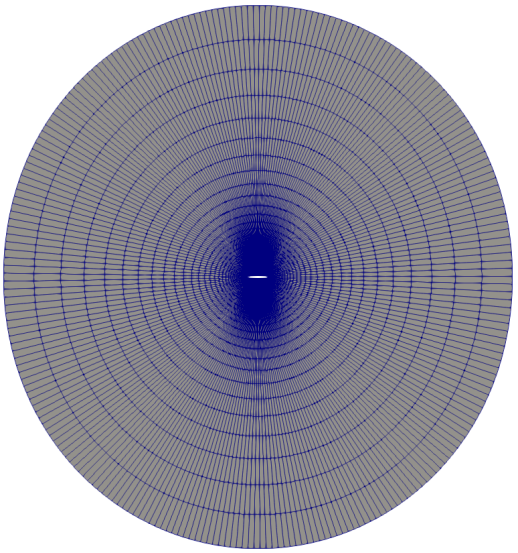

**(a)** Overall computational domain.

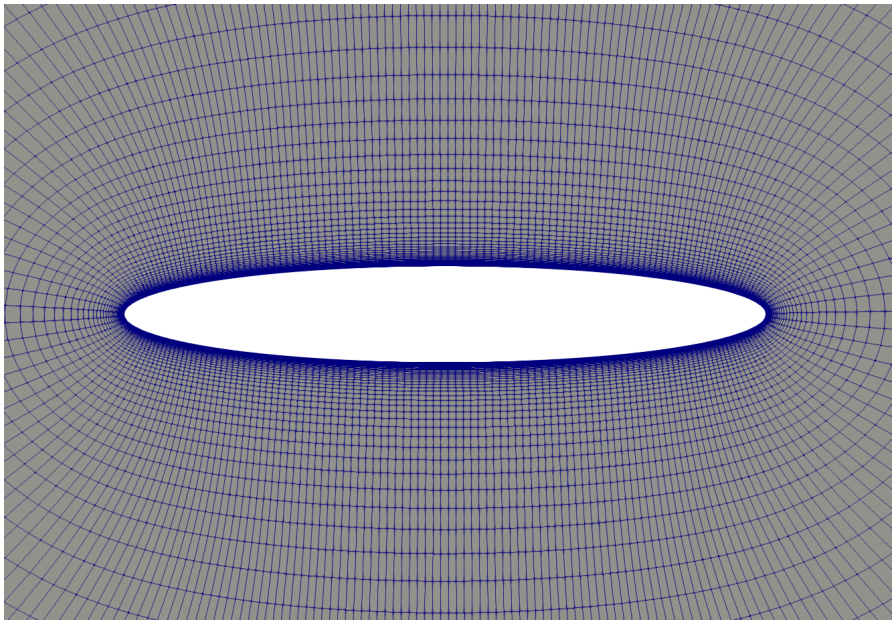

**(b)** Mesh near the airfoil.

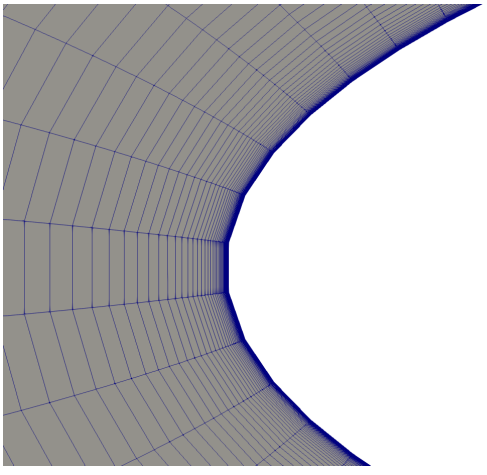

**(c)** Closeup near the leading edge.

**Figure 2.6:** Computational grid for the elliptic airfoil.

# Chapter 3

# Results

## 3.1 Elliptic airfoil

To validate the computational setup, the simulations for the elliptic airfoil was compared against experimental results from [15]. The lift coefficient over a range of angle of attacks are shown in Figure 3.1. The agreement is excellent in the lower range. However, the simulations predict stall earlier than the experiments. This is considered acceptable for the current work.

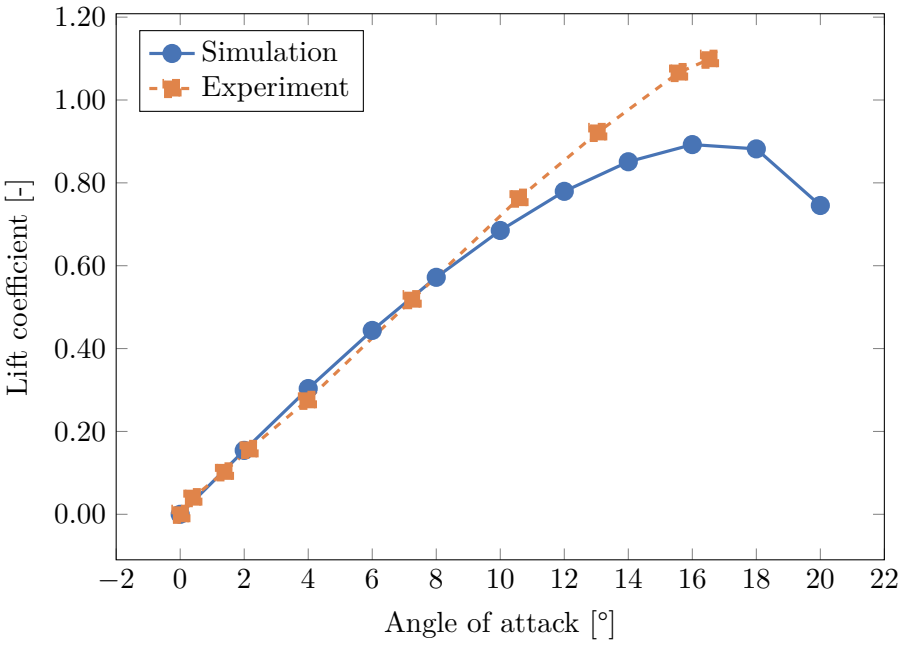


**Figure 3.1:** Simulated lift coefficients for elliptic airfoil, compared against experimental results[15].

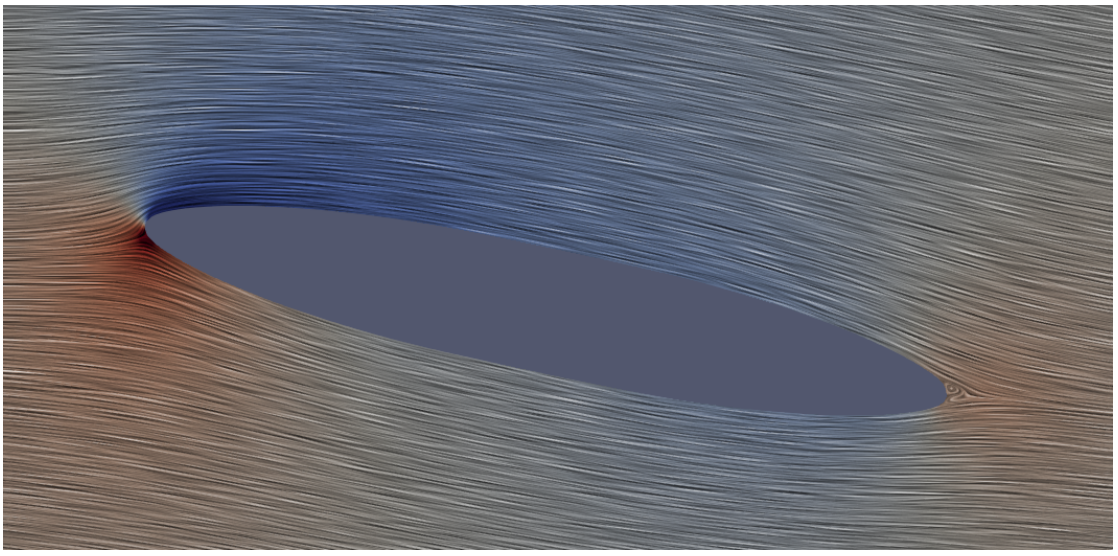

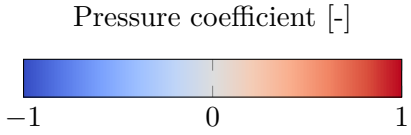


**(a)** Pressure coefficient and flow pattern for an angle of attack of 6 degrees.

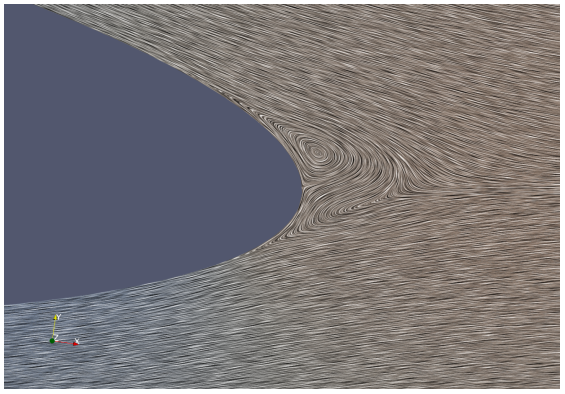

**(b)** Close-up near trailing edge showing flow separation.

**Figure 3.2:** Close-up near trailing edge showing flow separation.

As a representative illustration of the flow pattern around the airfoil, Figure 3.2 shows results for angle of attack equal to six. The colors indicate the pressure coefficient while the flow direction is visualized using line integral convolution. The lift is clearly seen by the low pressure on the top side of the airfoil and the high pressure on the lower side. An issue with the elliptic airfoil is also seen in the close-up near the trailing edge also shown in the figure. There is clear flow separation and recirculation here, which will cause a higher drag compared to the thinner trailing edge of a typical unidirectional airfoil.

The behavior after stall, at angle of attack equal to 20, is shown in Figure 3.3. Here, there is a large separation zone over most of the upper part of the airfoil severly reducing the performance of the airfoil.

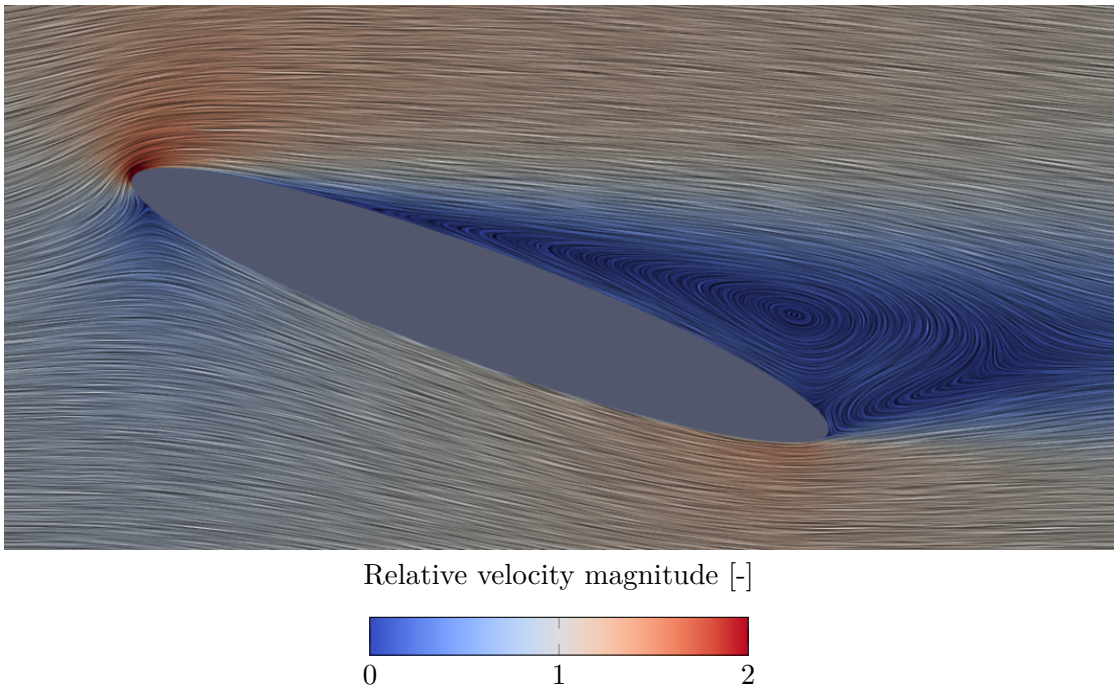


**Figure 3.3:** Flow pattern at 20 degrees angle of attack, showing stall behavior with severe separation.

## 3.2 Bisymmetric NACA airfoil, SYM65-015

The lift coefficient for the bisymmetric version of the baseline airfoil is shown in Figure 3.4. The performance is almost identical to the ellipsoid airfoil. This is expected given the highly similar geometry.

## 3.3 Reversible NACA airfoil, REV65-415

The lift coefficient for the reversible version of the baseline airfoil is shown in Figure 3.5. Here, results for the baseline airfoil and the bisymmetric airfoil are also included for comparison. Both the bisymmetric and the asymmetric reversible airfoils have significantly lower lift coefficients compared to the baseline airfoil.

The asymmetric airfoil is slightly better than the symmetric airfoil at lower angles of attack. However, it also stalls earlier. A comparison of the flow patterns are angle of attack equal to 14 is shown in Figure 3.6. There is clearly a higher degree of separation near the trailing edge for the asymmetric airfoil.

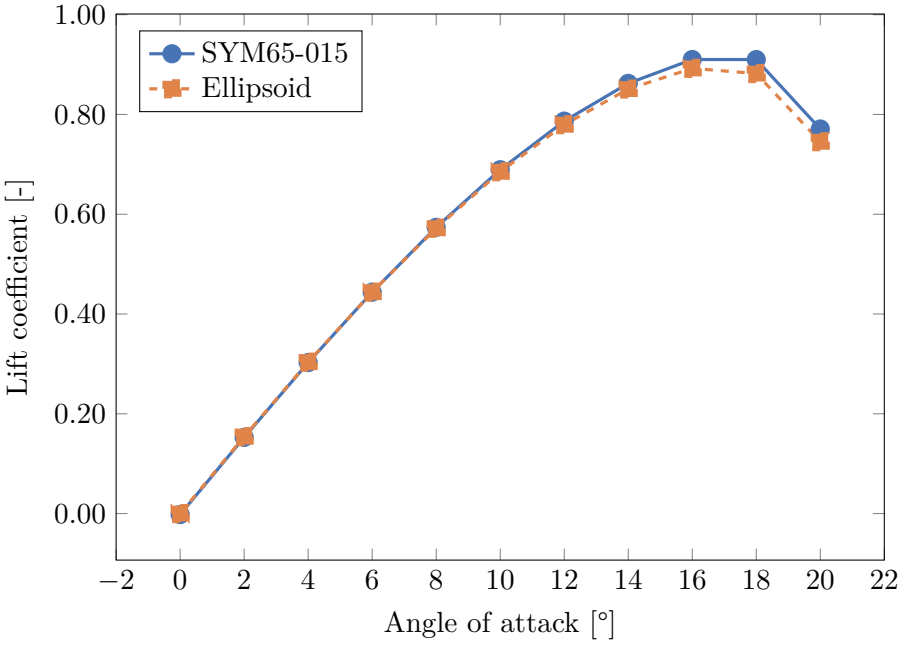


**Figure 3.4:** Simulated lift coefficients for the SYM65-015 airfoil, compared against the ellipsoid airfoil.

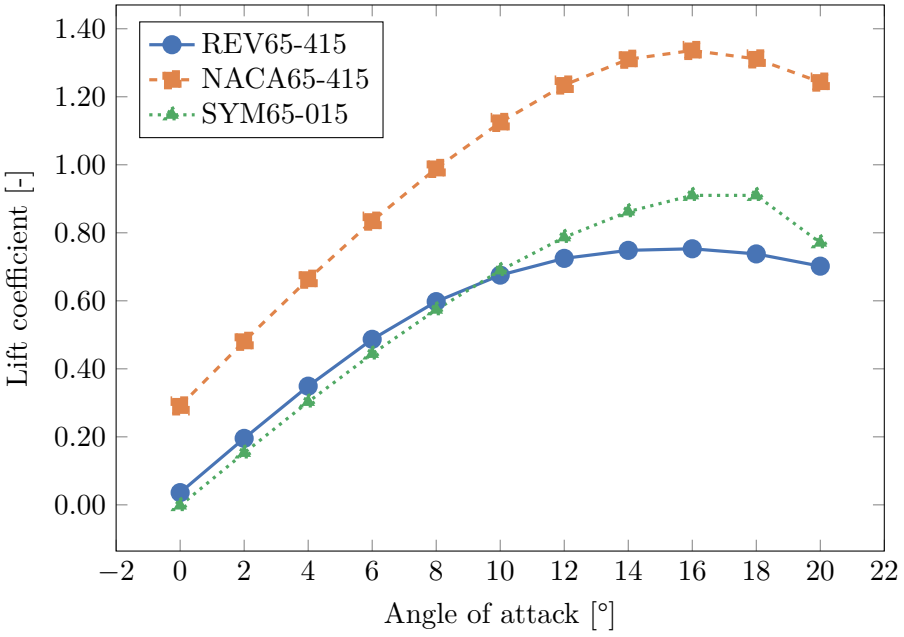


**Figure 3.5:** Simulated lift coefficients for the reversible version of the NACA65-415 airfoil, compared against the symmetric version and the actual airfoil.

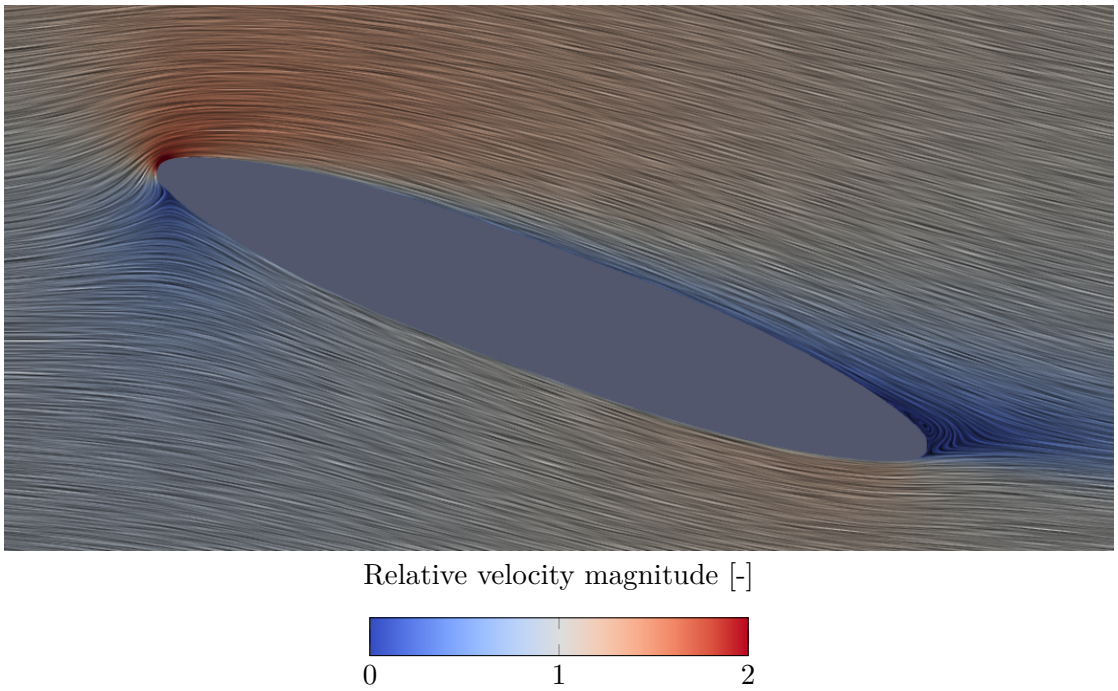


**(a)** SYM65-015

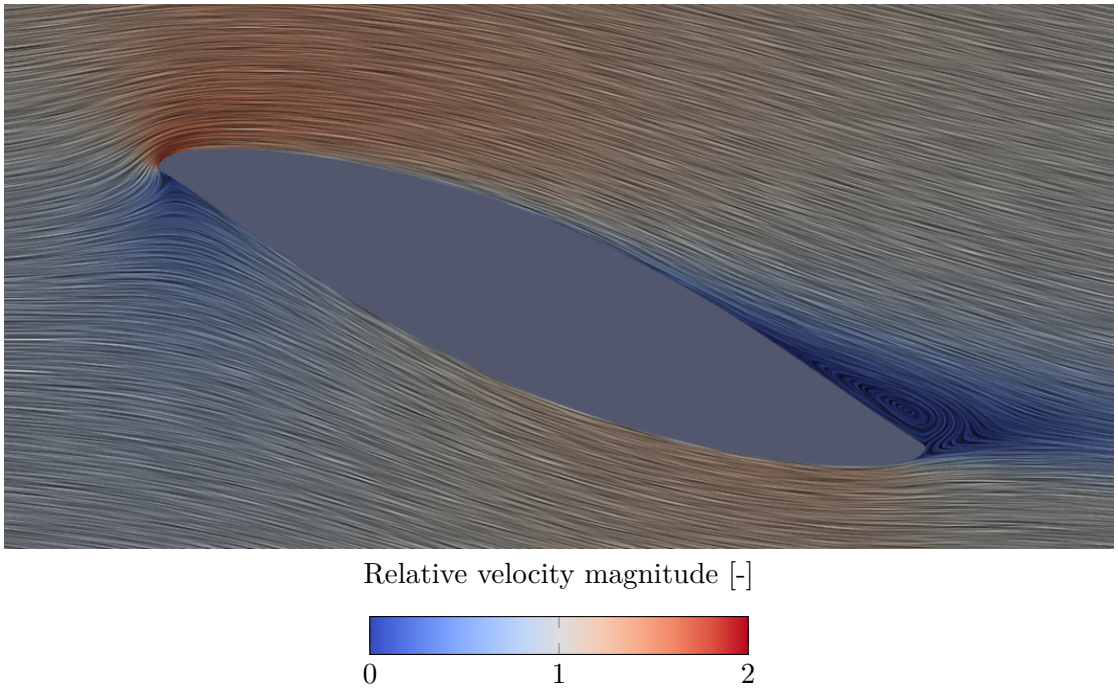


**(b)** REV65-015

**Figure 3.6:** Comparison of separation at 14 degrees angle of attack for the bisymmetric and reversible versions of the NACA 65-415 airfoil.

## 3.4 Optimized B-spline airfoils

### 3.4.1 Lift

In the first experiment, the objective function is chosen to be the lift coefficient. Only a single angle of attack of 6 degrees is considered.

The development of the objective function along with the control points is shown in Figure 3.7. There is a quick increase in the lift followed by a slow gradual increase until the value stabilizes after around 200 iterations. The best design gives $C_L = 1.23$.

The resulting airfoil is shown in Figure 3.8. Also shown is a second airfoil where the blunt edge is manually adjusted to be slightly less blunt. Optimizing at a single angle of attack and with only lift as the objective function gives very thick and blunt profiles. This will increase the projected area of the pressure side of the airfoil that the incoming water sees and thereby increase the lift. However, this also results in a blunt leading edge on the suction side, which increases the drag and also leads to stall earlier than a leaner profile. This is shown in Figure 3.9a, which shows the lift for the two airfoils compared against the bisymmetric airfoil. The lift coefficient for the optimized airfoil rapidly drops after the optimization point, indicating that a single point for the optimization is not sufficient. The manually adjusted profile has lower maximum lift, but also goes into deep stall later than the optimized airfoil. The lift is significantly higher than the bisymmetric airfoil. However, until now only lift has been considered. Drag is also an important element of the performance of an airfoil. Figure 3.9 shows the lift-to-drag ratio, often called the aerodynamic effectiveness. This plot shows that the effectiveness is lower than the bisymmetric airfoil over a large range of angles of attack.

### 3.4.2 Lift/drag ratio

The next test was done by looking at aerodynamic efficiency, i.e. lift-to-drag ratio, as the objective function. Still, only a single angle of attack was considered.

The development of the objective function and the control points is shown in Figure 3.10. A stable maximum is reached after around 50 iterations. The resulting airfoil is shown in Figure 3.11. Optimizing with respect to the aerodynamic effectiveness gives a very thin profile. From the resulting drag and lift coefficients, as seen in Figure 3.12, it is clear that the optimization gives good results at the optimization point but quickly falls off away from it. Additionally, a very thin profile will gives issues with structural performance and manufacturing.

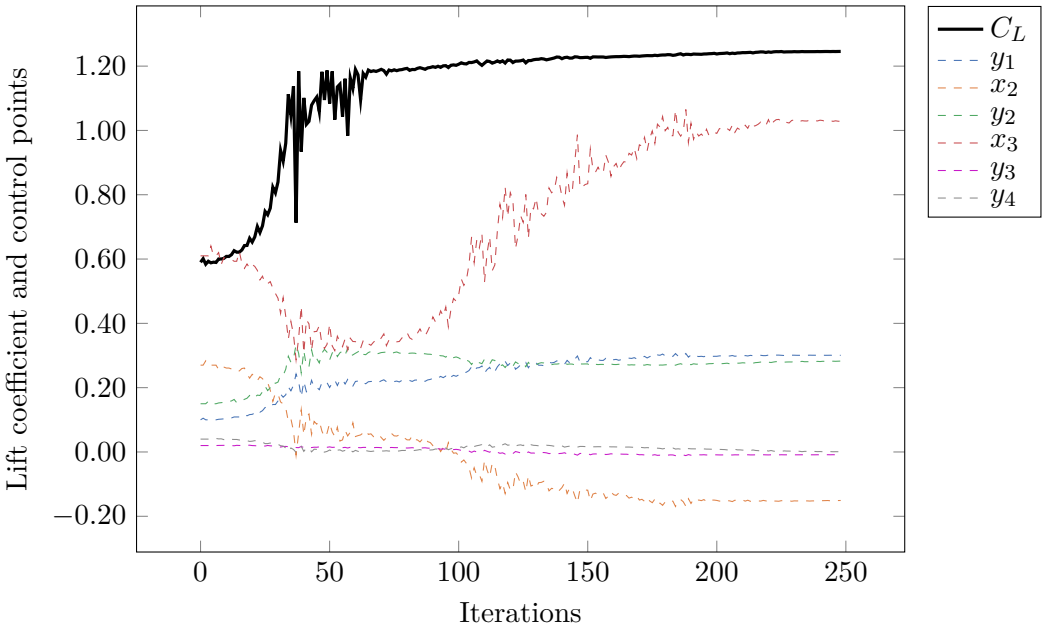


**Figure 3.7:** Development of objective function (lift) and control point location for the optimization at a single angle of attack.

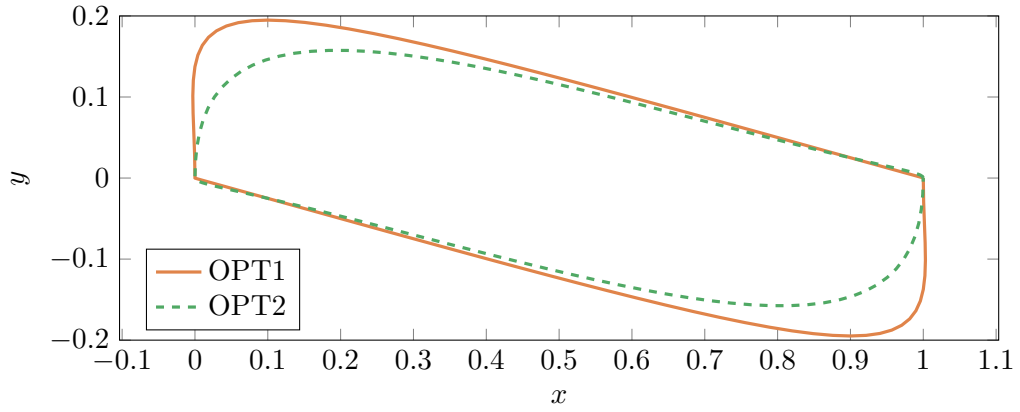


**Figure 3.8:** The resulting airfoils for the optimization of lift at a single angle of attack.

### 3.4.3 Multipoint lift/drag ratio

A deficiency of the previous approach was that the performance of the resulting airfoil quickly deteriorates beyond the considered angle of attack. Here, multiple points are introduced in attempt to alleviate this problem. The objective function chosen is

$$\text{OBJ} = \frac{3}{2}\alpha_{AoA=6} + \alpha_{AoA=12} \tag{3.1}$$

The 1.5 factor in front of the lowest angle of attack is introduced to make sure the two points will have a similar weighting in the optimization process.

The development of the objective function and the control points is shown in Figure 3.13.

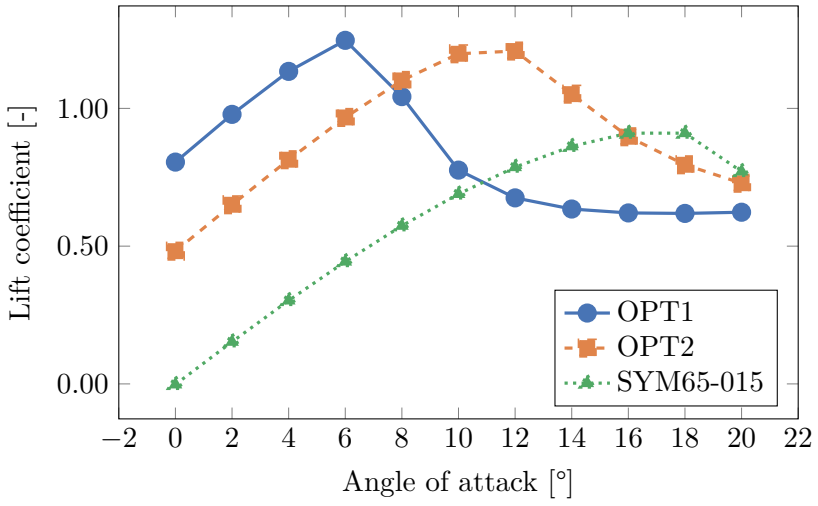


**(a)** Lift coefficient.

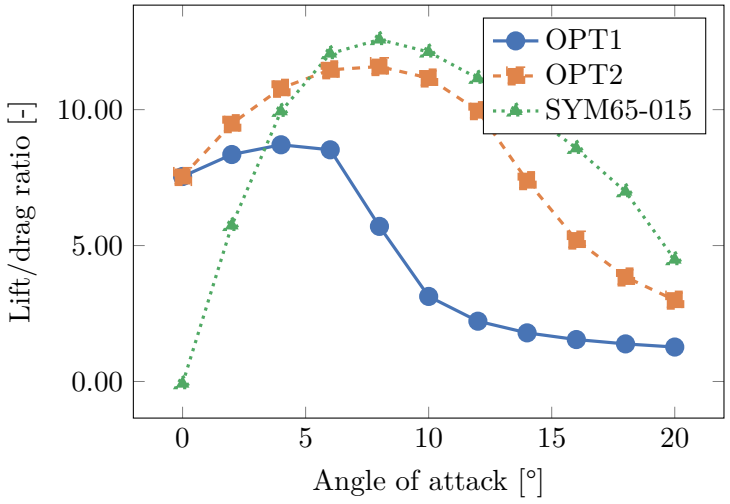


**(b)** Lift-to-drag ratio.

**Figure 3.9:** Results for the airfoils optimized with respect to lift at a single angle of attack of six degrees.

A stable maximum is reached after around 60 iterations. The resulting airfoil is shown in Figure 3.14. This is less extreme than the airfoil from optimizing at a single angle of attack, but is still a relatively thick airfoil with a blunt nose.

The lift coefficients and lift-to-drag ratios are shown in Figure 3.15. The lift coefficient is significantly improved compared to the bisymmetric profile. The early dropoff found from the airfoil optimized at a single angle of attack is also reduced, and the aerodynamic effectiveness is comparable to the bisymmetric design.

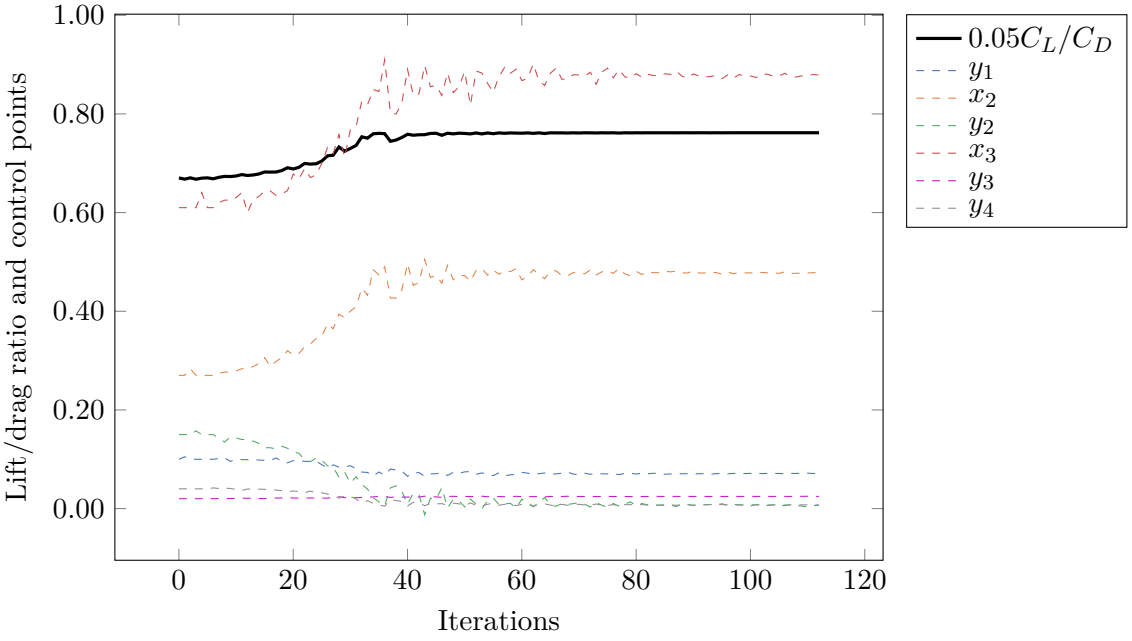


**Figure 3.10:** Development of objective function (lift/drag ratio) and control point location for the optimization at a single angle of attack.

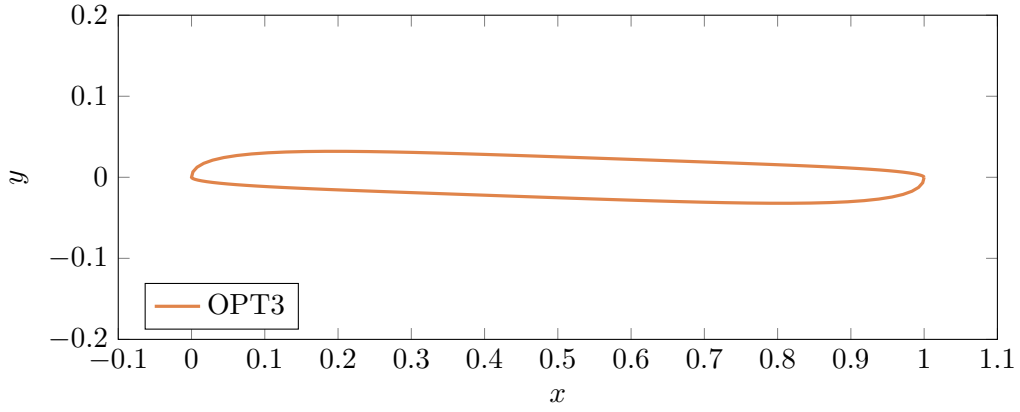


**Figure 3.11:** The resulting airfoils for the optimization of lift/drag ratio at a single angle of attack.

## 3.5 New airfoil designs

Taking the knowledge gained from the optimization tests, a final design was made by hand. The airfoil should have sufficient thickness for the structural design, thin enough to have a good aerodynamic effectiveness but with a blunt edge to get a high lift coefficient. The airfoil is shown in Figure 3.16, and the coefficients in Figure 3.17. The design gives both improved lift and improved lift-to-drag ratio compared to the bisymmetric profile.

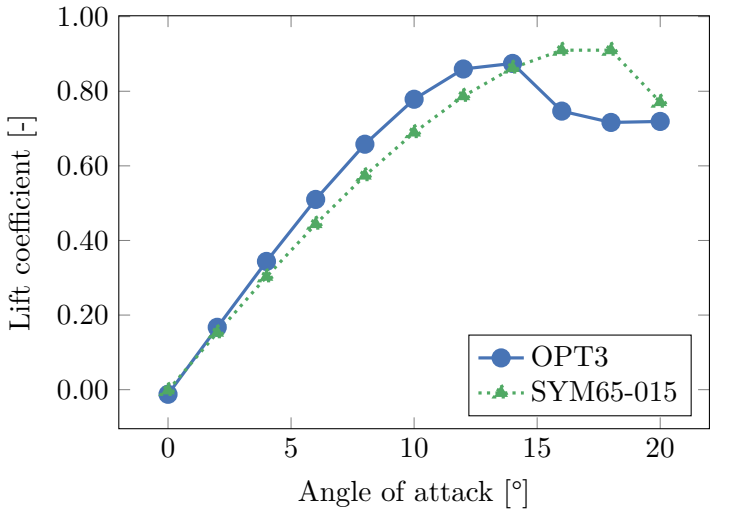


**(a)** Lift coefficient.

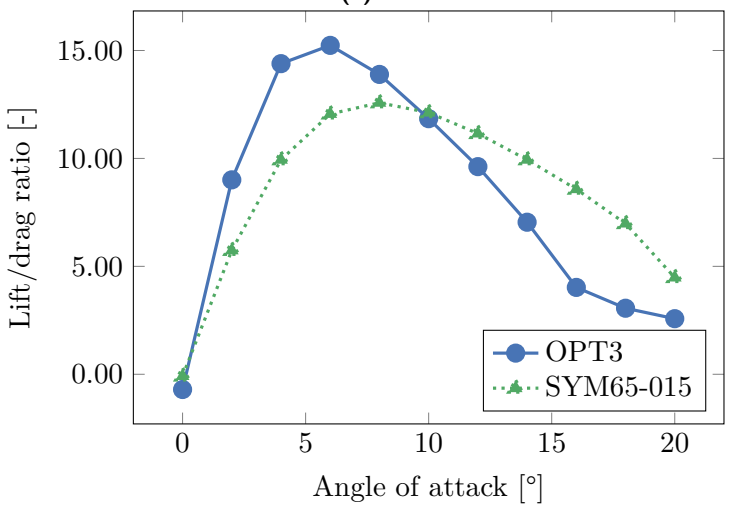


**(b)** Lift-to-drag ratio.

**Figure 3.12:** Results for the airfoils optimized with respect to lift/drag ratio at a single angle of attack of six degrees.

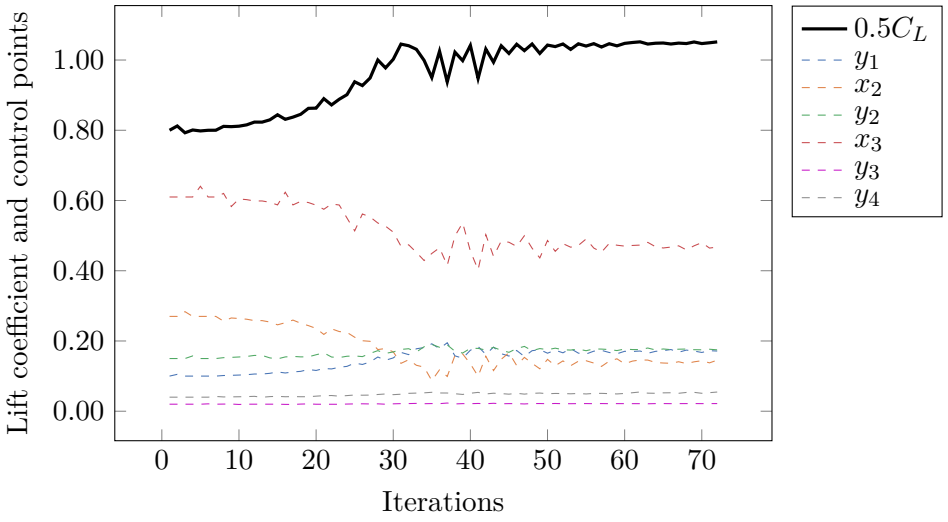


**Figure 3.13:** Development of objective function (lift) and control point location for the optimization at two angles of attack.

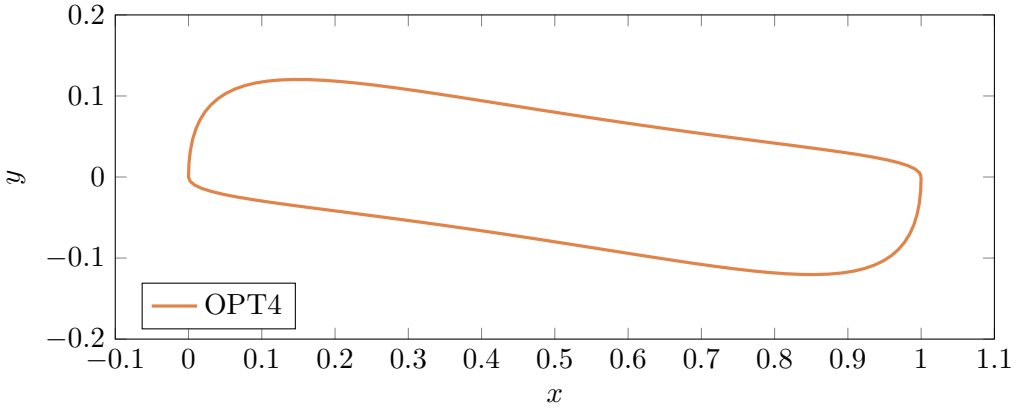


**Figure 3.14:** The resulting airfoils for the optimization of lift/drag ratio at two angles of attack.

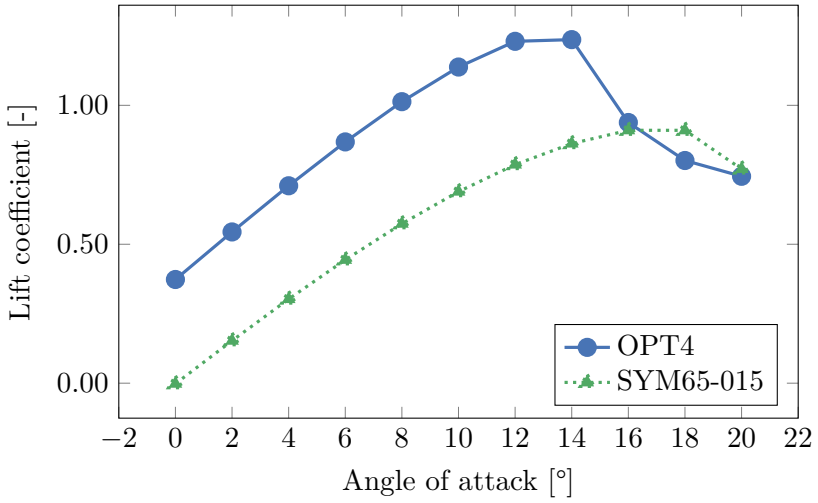


**(a)** Lift coefficient.

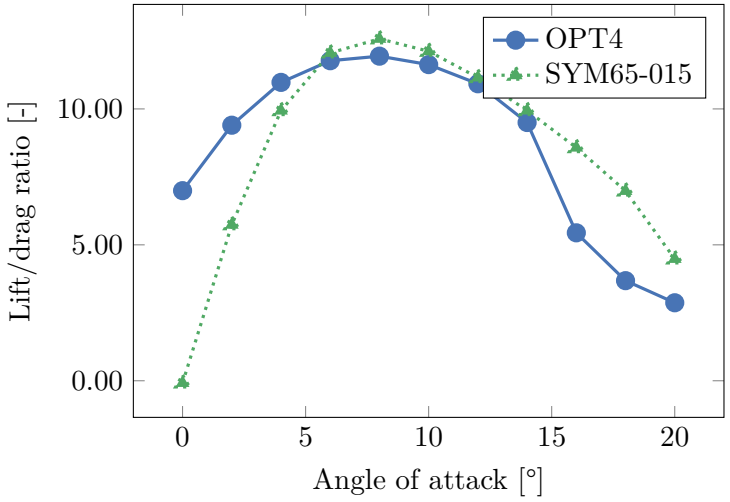


**(b)** Lift-to-drag ratio.

**Figure 3.15:** Results for the airfoils optimized with respect to lift at two angles of attack.

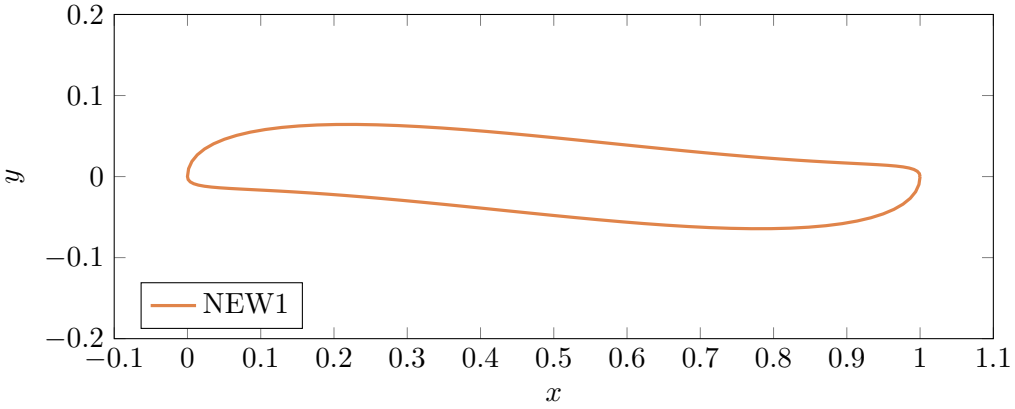


**Figure 3.16:** Airfoil designed based on knowledge gained from the optimization process.

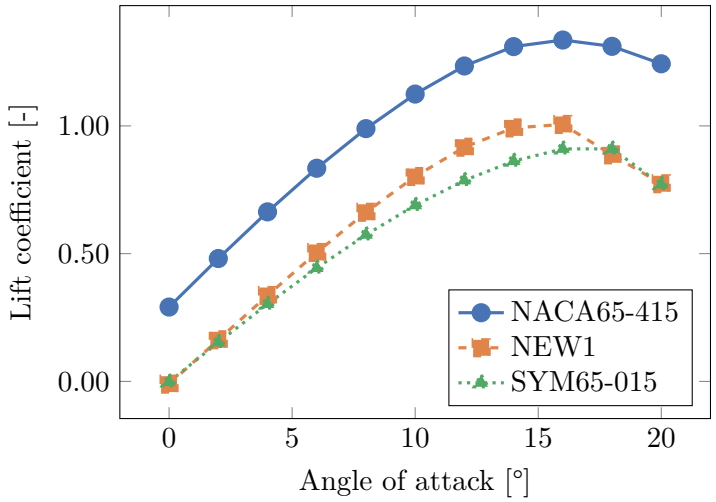


**(a)** Lift coefficient.

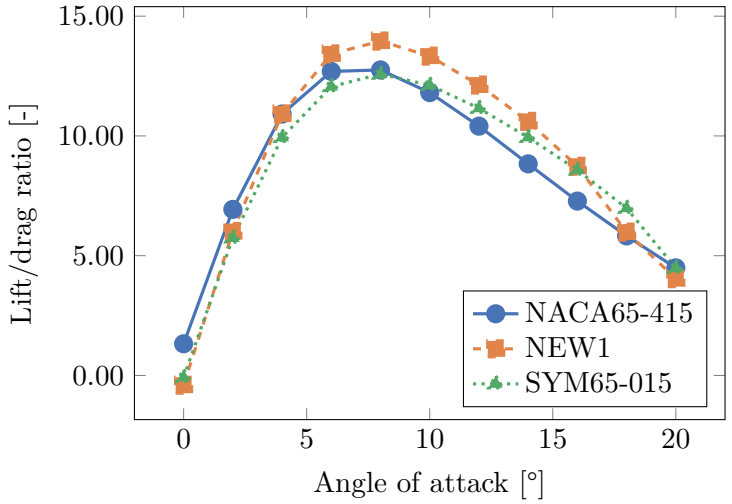


**(b)** Lift-to-drag ratio.

**Figure 3.17:** Results for the airfoil designed based on knowledge gained from the optimization process.

# Chapter 4

# Discussion and conclusions

This work investigated reversible airfoils for using in tidal turbines. Some airfoils were created based on a baseline airfoil from the NACA 6 series. Next, an airfoil parameterization was created using B-splines. An efficient CFD methodology was devised and used in an optimization prcocess. The results showed that an elliptic airfoil and the bisymmetric airfoil based on the NACA 6 profile had similar performance. The reversible, asymmetric NACA 6 profile had slightly better lift, but also stalled earlier than the elliptic airfoil. The optimization process showed that to get high lift for a reversible airfoil, a bluff leading edge is beneficial as this increases the area of the exposed pressure side of the airfoil. However, this also leads to high drag and poor stall performance. Optimizing with respect to lift-to-drag ratio gave very thin profiles. A new design was made by hand was made based on the optimized designs. This new design had both improved lift and improved aerodynamic effectiveness compared to the elliptic airfoil.

Airfoil optimization is a complex topic, and it is difficult to find a method that will give a perfect airfoil. There are many considerations to be made regarding parametrization, choice of objective function, choice of solvers and so on. However, optimization is a viable tool to gain insights into the airfoil performance. By having sufficiently cheap evaluation of the objective function and the overall optimization algorithm, optimization can be part of an iterative design process to arrive at airfoils that are an improvement on simpler designs and that satisfy a wide range of operational requirements.

Future work should consider optimizing with constraints and multi-objective optimization. For instance, by optimizing with lift and drag as objectives, the Pareto front could be found further demonstrating the compromise between these two quantities for a reversible airfoil. As constraints, the thickness of the profile could be a relevant parameter, or the stall performance. Finally, the resulting aerodynamic coefficients should be put into a

model simulating a full tidal turbine design to get the complete view of the performance of the proposed airfoils.

# List of Figures

# List of Tables

# Bibliography


[1] Sanya Carley. State renewable energy electricity policies: An empirical evaluation of effectiveness. *Energy Policy*, 37:3071–3081, 04 2011. doi: 10.1016/j.enpol.2009.03.062.

[2] Nasir Mehmood, Zhang Liang, and Jawad Khan. Harnessing ocean energy by tidal current technologies. *Research Journal of Applied Sciences, Engineering and Technology*, 4, 09 2012.

[3] Fergal O Rourke, Fergal Boyle, and Anthony Reynolds. Tidal energy update 2009. *Applied energy*, 87(2):398–409, 2010.

[4] Noor Rahman, Saeed Badshah, Abdur Rafai, and Mujahid Badshah. Literature review of ocean current turbine. *International Journal of Scientific & Engineering Research*, 5(11):11, 2014.

[5] PR Cave and EM Evans. Tidal stream energy systems for isolated communities. In *Alternative Energy Systems*, pages 9–15. Elsevier, 1984.

[6] Nilesh P. Salunke, Juned Ahamad R. A., and S.A. Channiwala. Airfoil parameterization techniques: A review. *American Journal of Mechanical Engineering*, 2(4): 99–102, 2014.

[7] Gino Angelini, Tommaso Bonanni, Alessandro Corsini, Giovanni Delibra, Lorenzo Tieghi, and David Volponi. On surrogate-based optimization of truly reversible blade profiles for axial fans. *Designs*, 2(2):19, 2018.

[8] Mark Drela. Pros and cons of airfoil optimization. *Frontiers of computational fluid dynamics*, 1998:363–381, 1998.

[9] John A Nelder and Roger Mead. A simplex method for function minimization. *The computer journal*, 7(4):308–313, 1965.

[10] Saeed Badshah, Mujahid Badshah, Noman Hafeez, Sakhi Jan, and Zia Ur Rehman. Cfd analysis of tidal current turbine performance with different boundary conditions. In *IOP Conference Series: Earth and Environmental Science*, volume 581, page 012010. IOP Publishing, 2020.

[11] Henry G Weller, Gavin Tabor, Hrvoje Jasak, and Christer Fureby. A tensorial approach to computational continuum mechanics using object-oriented techniques. *Computers in physics*, 12(6):620–631, 1998.

[12] Hrvoje Jasak, Aleksandar Jemcov, Zeljko Tukovic, et al. Openfoam: A c++ library for complex physics simulations. In *International workshop on coupled methods in numerical dynamics*, volume 1000, pages 1–20. IUC Dubrovnik Croatia, 2007.

[13] Philippe Spalart and Steven Allmaras. A one-equation turbulence model for aerodynamic flows. In *30th aerospace sciences meeting and exhibit*, page 439, 1992.

[14] Peter K Sweby. High resolution schemes using flux limiters for hyperbolic conservation laws. *SIAM journal on numerical analysis*, 21(5):995–1011, 1984.

[15] S. F. Hoerner and H. V. Borst. Fluid-dynamic lift: Practical information on aerodynamic and hydrodynamic lift. *NASA STI/Recon Technical Report A*, 76: 32167, May 1975.